Applied Surface Science 258 (2012) 3393–3404

Contents lists available at SciVerse ScienceDirect

Applied Surface Science

journal homepage: www.elsevier.com/locate/apsusc

Resistivity of thin gold films on mica induced by electron–surface scattering: Application of quantitative scanning tunneling microscopy

Marcelo E. Robles[a], Claudio A. Gonzalez-Fuentes[b], Ricardo Henriquez[b], German Kremer[c], Luis Moraga[b], Simón Oyarzun[b], Marco Antonio Suarez[b], Marcos Flores[b], Raul C. Munoz[b,*]

[a] Departamento de Ciencias de la Construcción, FCCyOT, Universidad Tecnológica Metropolitana, Dieciocho 390, Santiago 8330526, Chile
[b] Departamento de Física, Facultad de Ciencias Físicas y Matemáticas, Universidad de Chile, Blanco Encalada 2008, Casilla 487-3, Santiago 8370449, Chile
[c] Departamento de Física, Facultad de Ciencias, Universidad de Chile, Las Palmeras 3425, Santiago 7800024, Chile

ARTICLE INFO

Article history:
Received 12 May 2011
Received in revised form 6 October 2011
Accepted 8 November 2011
Available online 26 November 2011

Keywords:
Resistivity induced by electron-surface scattering
Classical theories and quantum theories of size effects
Surface roughness measured with a STM
Parameters describing the surface roughness
rms roughness amplitude and lateral correlation length

PACS:
73.50.−h
73.61.−r

ABSTRACT

We report a comparison between the resistivity measured on thin gold films deposited on mica, with predictions based upon classical theories of size effects (Drude's, Sondheimer's and Calecki's), as well as predictions based upon quantum theories of electron–surface scattering (the modified theory of Sheng, Xing and Wang, the theory of Tesanovic, Jaric and Maekawa, and that of Trivedi and Aschroft). From topographic images of the surface recorded with a Scanning Tunneling Microscope, we determined the rms roughness amplitude, δ and the lateral correlation length, ξ corresponding to a Gaussian representation of the average height–height autocorrelation function, describing the roughness of each sample in the scale of length set by the Fermi wave length. Using (δ, ξ) as input data, we present a rigorous comparison between resistivity data and predictions based upon the theory of Calecki as well as quantum theoretical predictions *without adjustable parameters*. The resistivity was measured on gold films of different thickness evaporated onto mica substrates, between 4 K and 300 K. The resistivity data covers the range $0.1 < x(T) < 6.8$, for $4\,K < T < 300\,K$, where $x(T)$ is the ratio between film thickness and electron mean free path in the bulk at temperature T. We experimentally identify electron–surface and electron–phonon scattering as the microscopic electron scattering mechanisms giving rise to the macroscopic resistivity. The different theories are all capable of estimating the thin film resistivity to an accuracy better than 10%; however the mean free path and the resistivity characterizing the bulk turn out to depend on film thickness. Surprisingly, only the Sondheimer theory and its quantum version, the modified theory of Sheng, Xing and Wang, predict and increase in resistivity induced by size effects that seems consistent with published galvanomagnetic phenomena also arising from electron–surface scattering measured at low temperatures.

1. Introduction

One of the fundamental problems in Solid State Physics that has attracted the attention of researchers for over a century [1], relates to the effect that electron scattering by defects such as grain boundaries and rough surfaces has on charge transport in metallic nanostructures. A central issue is how the surface of the structure affects electrical transport, when one or more of the dimensions characterizing the structure are comparable to or smaller than the mean free path of the charge carriers in the bulk, what has become known as size effects. The miniaturization effort pursued by the electronic industry worldwide posses a pressing need to understand and eventually to predict how electron–surface scattering induces an increase in the resistivity of metallic nanostructures. The technical importance of this problem is reflected in the fact that it has sparked a debate over the last decade within the semiconductor industry [2], and has given rise to several papers focused on this issue published over the last two years [3–11]. However, after over a century of research, the understanding of size effects in thin metallic films today still seems fragmentary and incomplete.

On the one hand, Graham and co-workers [9] recently reported the room temperature resistivity of sub 50 nm Cu wires, where the resistivity of the wires seems determined by electron–surface plus electron–phonon scattering; electron-grain boundary scattering in this case seems to play a minor role. On the other hand, Sun and co-workers [10] reported on the resistivity of some 22 Cu films of different thickness measured at 4 K and at 296 K, where the samples are made out of grains of different size, and the resistivity data at room temperature is interpreted as being dominated by electron-grain boundary scattering plus electron–phonon scattering, and it

* Corresponding author. Tel.: +56 2 978 4335.
E-mail address: ramunoz@ing.uchile.cl (R.C. Munoz).

0169-4332/$ – see front matter © 2011 Elsevier B.V. All rights reserved.
doi:10.1016/j.apsusc.2011.11.035

is assumed that electron-grain boundary scattering is characterized in *all* samples by the same grain boundary reflectivity *R*. These two reports and the discussions published by the semiconductor industry [12] reflect what appears to be incomplete understanding.

The reason that might explain such fragmentary and incomplete understanding may be related to the fact that, quite often, there are several electron scattering mechanisms at work, and the identification of the different electron scattering mechanisms participating in charge transport is a rather complex and subtle issue; such identification can rarely be obtained from simply measuring the resistivity of the samples. The results published in Ref. [10] constitute a strong evidence that supports a suggestion published over 25 years ago [13], and confirms that the contribution to the resistivity of a thin metallic film arising from electron scattering by structural defects other than rough surfaces (such as electron-grain boundary scattering) may be significant [10,11,13]. Regarding measurements and the interpretation of thin film resistivity data as arising from electron–surface scattering, this evidence raises the necessity of performing additional experiments aimed at verifying that the observed resistivity is controlled, indeed, by electron–surface plus electron–phonon scattering, and is not dominated by some other structural defects present in the samples.

Regarding the theoretical description of size effects, there are theories based upon a classical description of electron motion provided by a Boltzmann Transport Equation (BTE), and there are quantum theories published over the last fifteen years based upon Quantum Field Theory applied to Solid State Physics. Among the theories based upon a BTE there is the pioneering work of Sondheimer [14] that contains some (phenomenological) adjustable parameters, and the theory of Calecki [15], that contains no adjustable parameters.

On the other hand, quantum theories of size effects contain no adjustable parameters, and predict the film resistivity as a function of the parameters that statistically describe the roughness of the surface of metallic films. The quantum description of charge transport suggests that the relevant scale of length concerning electron–surface scattering, is set by the Fermi wave length λ_F of the charge carriers, which for several metals is in the scale of nanometers. Therefore, the relevant corrugations that should mainly determine the increase in resistivity arising from electron–surface scattering are those taking place over a scale of length comparable to λ_F to within an order of magnitude.

This suggestion emerging from quantum transport theories has some severe practical consequences. To compare thin film resistivity data with the predictions of either Calecki's classical theory, or with predictions based upon quantum theories, the surface roughness must be measured on each sample within the scale of length set by λ_F, together with its resistivity. *Quantum theoretical predictions have not yet been tested against experimental data, other than by guessing the parameters that describe surface roughness, or by using the parameters contained in the models simply to fit the thin film resistivity data*.

Except for some exploratory work preformed a few years ago by our own group [16–20], experiments involving *both resistivity as well as surface roughness measured on each sample within the scale of length set by* λ_F have not been published. The most recent study of size effects in the resistivity of thin gold films [21], did not report independent measurements of surface roughness, the authors used classical theories to describe the resistivity data. Consequently, the question of how large the increase in resistivity of a thin metallic film attributable to electron–surface scattering at a given temperature really is—over and above the resistivity expected from the bulk (assuming that the resistivity arising from structural defects other than rough surfaces can be neglected), and how the predictions based upon quantum theories that contain no adjustable parameters compare with thin film resistivity data—remains open. One way to answer this open question is by comparing thin film resistivity data with quantum predictions once adjustable parameters have been eliminated from the model, by measuring the surface roughness of each specimen via a Scanning Probe Microscope capable of atomic resolution.

In this paper we report such a comparison: We report the temperature and the thickness dependence of the resistivity of a family of thin gold films deposited onto preheated mica substrates, measured at temperatures T ranging from $4\,K < T < 300\,K$, in samples that have been prepared such that *at 4 K electron–surface scattering is the dominant electron scattering mechanism*. In order to eliminate adjustable parameters from the different models, we measured the surface topography of each sample employing a Scanning Tunneling Microscope (STM). From the topography measured with the STM we determined the parameters that describe the surface roughness of each specimen in the scale of length set by λ_F (in gold, $\lambda_F = 0.52\,nm$). Here we report the first rigorous comparison between quantum theoretical predictions of size effects and thin film resistivity data *that relies on quantitative Scanning Tunneling Microscopy, using no adjustable parameters*.

2. Experimental

We prepared gold films on mica where the substrate temperature, evaporation rate and post evaporation annealing temperature used for sample preparation, were chosen such that the scattering mechanism controlling the resistivity of the films at 4 K can be univocally identified as electron–surface scattering. To achieve this goal and to minimize the contribution to the resistivity of the films arising from electron scattering by defects other than rough surfaces (such as electron-grain boundary scattering), we relied on results of some exploratory experiments already published.

In Ref. [22] we reported the resistivity of a family of gold films of about the same thickness (54 nm) made out of grains whose average diameter D varies from some 11 nm to some 110 nm. The resistivity data was analyzed in terms of an updated version of the theory of Mayadas and Shatzkes that includes two surfaces with different specularities. In this experiment *we maped out, experimentally, the region where electron-grain boundary scattering plays a significant role in gold films*. It turns out that the contribution to the resistivity arising from electron-grain boundary scattering is dominant in samples where the mean grain diameter D is comparable to or smaller than $\ell_0\,(300) = 38\,nm$, the electronic mean free path in crystalline gold at 300 K. *For films where D is 100 nm or larger, the experimental result indicates that the effect of electron grain boundary scattering on the film resistivity can be safely neglected* [22].

This is confirmed by independent experiments reported in Ref. [23], where we report the Hall effect arising from electron–surface scattering. We showed that when $D > 100\,nm$, the Hall mobility measured at 4 K increases linearly with film thickness t, something that is also reported in Fig. 2 of Ref. [22]. A linear dependence between the electron collision time (which is proportional to the Hall mobility) and the film thickness *constitutes the finger print that allows univocal identification of electron–surface scattering being the dominant electron scattering mechanism at 4 K*, and it indicates, indeed, that the effect of electron-grain boundary scattering is negligible.

Based upon these experiments, we selected the sample preparation method. We used gold pellets 99.9999% pure evaporated at 3 nm/min from a tungsten basket filament onto freshly cleaved mica substrates in a high vacuum (HV) evaporation chamber (vacuum of 1.0×10^{-5} Pa during evaporation). The thickness was monitored in situ during the deposition by a quartz microbalance. To obtain samples where $D > 100\,nm$, the mica substrate was

Table 1
Morphological and electrical characterization of the samples. t: Sample thickness. D: average grain diameter (diameter of a circle enclosing the same area). ΔD: standard deviation of D. $\rho(300)$: resistivity at 300 K. $\rho(4)$: resistivity at 4 K. ℓ (4): average distance traveled by the electron at 4 K between scattering events, according to Drude's model.

t (nm))	D (nm)	ΔD (nm)	$\rho(300)$ (nΩ m)	$\rho(4)$ (nΩ m)	ℓ_0 (4) (nm)
54	109.7	43.9	32.7	7.6	110
96	159.7	43.1	29.9	4.09	205
135	179.2	64.9	25.9	2.58	325
255	130.2	30.8	23.3	1.68	499

preheated to 180 °C, and the films were annealed in HV for 1 h at 270 °C after evaporation. The morphology and structure of the samples was determined via X Ray Diffraction (XRD), Rutherford Back Scattering (RBS), and STM. The X-ray signal was recorded by an X-ray diffractometer operating in the θ–2θ mode, it indicates that the samples are made up of grains oriented such that direction <1 1 1> is perpendicular to the surface of the mica. The thickness of the samples was measured (to an accuracy of 5%) recording the RBS spectra of 2 MeV alpha particles from a Van der Graaff accelerator.

The resistivity of the films was measured between 4 K and 300 K (± 0.1 K) using the 4 point method, injecting a current of 1.3 mA and 210 Hz, and measuring the voltage drop across the samples by means of computer controlled Lock-in Amplifiers. The samples were inserted into a copper block in a superconducting magnet.

To obtain the parameters characterizing the roughness, the surface of each sample was recorded using a STM running in air, equipped with a Pt–Ir tip. Before recording data, we verified that the STM tip was capable of delivering atomic resolution over HOPG samples.

The morphological and electrical characteristics of the samples are summarized in Table 1. The temperature dependence of the resistivity of the samples is displayed in Fig. 1. The typical grain texture of the films, measured with the STM, is displayed in Fig. 2.

3. Theory: methods of data analysis

3.1. Application of quantitative scanning tunneling microscopy to measure the surface roughness

3.1.1. Average height–height autocorrelation function

From the raw data recorded with the STM, some precautions must be taken before extracting the surface roughness parameters that are to be used as input in theories of size effects. The height contained in each pixel on each image recorded by the STM, is measured with respect to a reference that may change from image to image. Moreover, the scanner most commonly is not oriented exactly normal to the plane of the film. Consequently, in order to eliminate artifacts from the images that could arise from slightly different orientation of the scanner relative to the surface of the sample, that would manifest as a tilt that may vary from image to image, it becomes necessary to apply a planar subtraction to each of the images recorded with the STM.

The surface of the samples exhibit rather flat areas that extend (along the plane of the film) over distances of several tens of nm (region labeled grain terraces, GT in Table 2 and Fig. 2), followed by steep planes (region labeled grain side, GS in Table 2 and Fig. 2), that join an adjacent grain (region labeled as grain boundary, GB in Table 2 and Fig. 2). In order to extract the roughness parameters relevant for electron scattering, we recorded 10 nm × 10 nm images containing 256 × 256 pixels in each of these three regions, on each sample, and applied a planar subtraction.

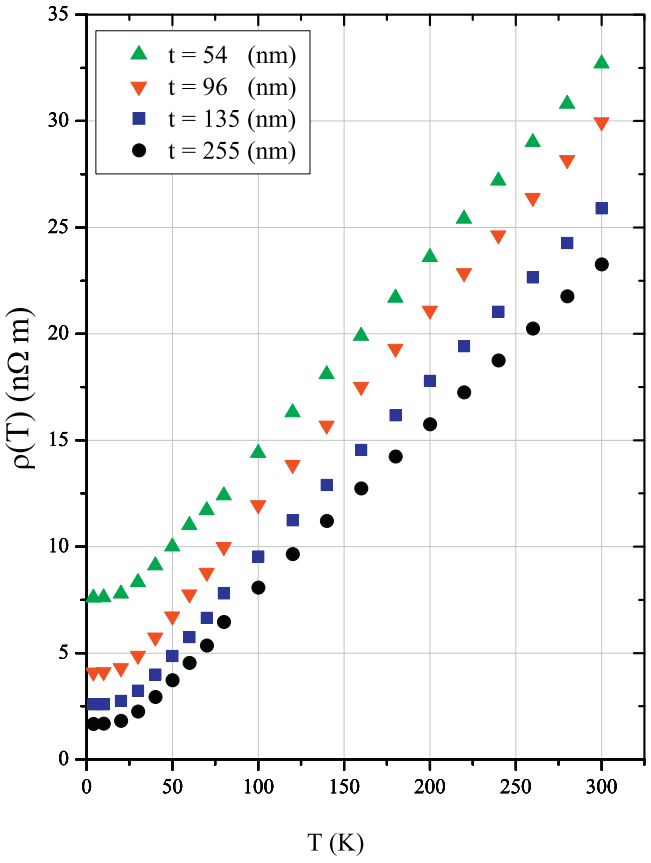

Fig. 1. Temperature dependence of the resistivity of 4 thin gold films deposited onto mica substrates.

The height–height surface ACF $f(r_{||}) = f(x, y)$ corresponding to each image, is defined by

$$f(r_{||}) = f(x,y) = S^{-1}\int_S h(a_{||})h(a_{||}+r_{||})d^2a_{||}, \quad (1)$$

where S denotes the surface sampled, $r_{||} = (x, y)$ stands for the in-plane coordinates and $h(a_{||})$ represents the random height characterizing the surface roughness. The integration is performed over the sample area S, assuming that the function $f(x, y)$ is continuous. The quantity measured with the STM is $h(a_{||})$. In the exploratory work published a few years ago, to compute $f(x, y)$ we used periodic boundary conditions imposed on $h(a_{||})$ on each image recorded with the STM [16,17]. Rather than following this procedure, in this

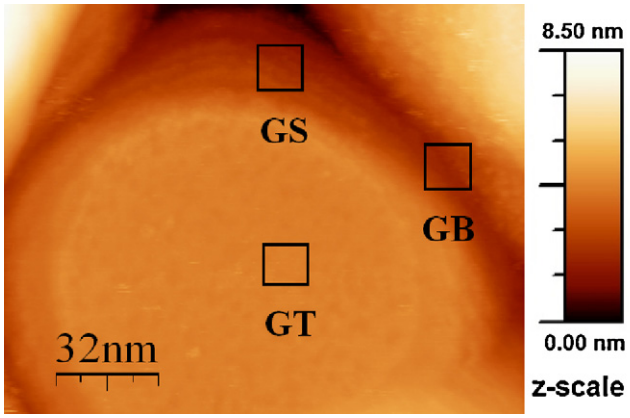

Fig. 2. Image of the surface of the 54 nm thick film, recorded with the STM, indicating grain texture: grain terrace (GT), grain side (GS) and grain boundary (GB).

Table 2
Parameters δ and ξ corresponding to a Gaussian representation of the ACF. t: Sample thickness. δ: rms roughness amplitude. ξ: lateral correlation length. c: additive constant, corresponding to a Gaussian representation of the autocorrelation function, considering the roughness parameters measured on different sites: grain terraces (GT), grain side (GS), and grain boundary (GB). The column χ^2/ν represents the goodness of the fit over more than ten thousand data points per sample, e.g. the statistical error χ^2 over the number of data points ν of the fit.

Site	t (nm)	δ (nm)	ξ (nm)	c (nm)	χ^2/ν
GT	54	0.05	1.8	0.00	1.0
	96	0.06	2.2	0.00	0.5
	135	0.06	1.5	0.00	0.5
	255	0.10	2.0	0.00	0.4
GS	54	0.10	2.7	0.00	0.3
	96	0.07	1.4	0.00	0.3
	135	0.05	1.4	0.00	1.4
	255	0.09	2.0	0.00	0.6
GB	54	0.38	3.3	−0.04	0.7
	96	0.42	3.9	−0.08	0.5
	135	0.48	3.5	−0.12	0.6
	255	0.46	2.3	−0.03	0.7

work we divided the area recorded with the STM into nine square sections containing an equal number of pixels each. The discrete version of the ACF corresponding to one STM image, is given by the summation

$$f(x_i, y_j) = \frac{1}{N \times N} \sum_{k,l=1}^{N} h(x_i + x_k, y_j + y_l) h(x_k, y_l) \quad (2)$$

where we chose $N = 256$ (for an image having 256×256 pixels), such that $-85 \le i \le +85$, $-85 \le j \le +85$. The inconvenience of this representation is that we obtain an experimental matrix representation of $f(x, y)$ that is discrete $f(x_i, y_j)$, of approximate dimensions $(2/3) \times (2/3)S$. This inconvenience is heavily outweighed by the fact that we do not assume any periodicity on the surface roughness data, a periodicity that the data does not support.

Although the ACF $f(x_i, y_j)$ corresponding to any particular STM image does not exhibit cylindrical symmetry (with respect to the z-axis perpendicular to the surface of the film), it is enough to average the ACF data over some 12–15 random images to obtain an ACF that approximately exhibits the required symmetry. To illustrate this fact we display in Fig. 3a and b the ACF of one individual image used to compute the average ACF recorded on a grain terrace of the 54 nm thick sample; the average ACF computed averaging over 12 images is displayed in Fig. 4.

It is interesting to note that such a cylindrical symmetry of the average ACF was assumed in the eighties and nineties in quantum theories describing the resistivity arising from electron–surface scattering. This assumption may be considered a consequence of the central limit theorem applied to the random sampling of the surface roughness, such as that displayed in Fig. 4. However, we do not know of any experimental verification of this assumption. We present in Fig. 4 the average surface ACF computed over some 12 images corresponding to different samples averaged over the grain terraces (GT), grain side (GS) and grain boundary (GB) of random grains making up each sample. The cylindrical symmetry of the experimental ACF is, indeed, restored by the averaging process.

3.1.2. Determination of the rms roughness amplitude and of the lateral correlation length, associated with a Gaussian representation of the ACF data

Before finding the appropriate Gaussian representation of the average ACF data obtained after performing the planar subtraction described, we must address a technical difficulty. A Gaussian representation of the ACF function $f_0(x, y) = \delta^2 \exp[-(x^2 + y^2)/\xi^2]$, leads to a function $f_0(x, y)$ that is always positive definite. Nevertheless, as shown in Fig. 3, the ACF corresponding to each STM image need not be positive definite, hence the experimental average ACF data (obtained after averaging the ACF computed on each image recorded with the STM, over a number of random images large enough to restore the cylindrical symmetry) need not be positive definite. The reason resides in the fact that the height recorded on each pixel of the images obtained with the STM, is measured with respect to a reference that may change from image to image. In order to accommodate this extra degree of freedom, we fitted a Gaussian of the form $f(x, y) = c + f_0(x, y)$, employing a least square fitting procedure with three fitting parameters: c, δ, ξ. In order to select the region over which the experimental, discrete ACF data $f(x_i, y_j)$ will be compared with its mathematical representation $f(x, y)$, we selected a circular area centered around the origin $(x_1, y_1) = (0, 0)$—the location where $f(x_i, y_j)$ attains its maximum value—an area whose radius was chosen as the average of the eight radii obtained by intersecting the curve $f(x_i, y_j) =$ zero with the eight directions oriented along the coordinate axis (x, y) plus directions differing by 45° from each other. The values obtained for c, δ and ξ, as well as the corresponding values for χ^2/ν describing the goodness of the fit over more than ten thousand data points for each sample, are listed in Table 2. The instrumental resolution of the STM equipped with a tip capable of delivering atomic resolution, is of the order of 12 pixels per C atom, or about $0.25\ \text{nm}/12 \approx 0.02$ nm. The values obtained for δ and ξ seem consistent with the instrumental resolution of the STM, scaled by $\sqrt{N}$, where $N > 10{,}000$ is the number of data points sampled for each ACF.

It seems remarkable that only 12–15 images are required to recover the cylindrical symmetry of the average ACF, and that the mathematical description of the ACF data by a Gaussian, is characterized by a typical statistical error χ^2/ν of the order of unity, over a set of ν data points that exceeds ten thousand data points for each ACF.

3.2. Determination of the bulk resistivity ρ_0 and bulk mean free path ℓ_0, using as input the surface roughness data

The residual resistivity (the temperature independent additive term appearing in the Bloch–Grüneisen theory describing the resistivity of crystalline metals) depends on the concentration of impurities/defects present in the crystal, and these concentrations do depend on the preparation of the crystal. On the other hand, the bulk resistivity $\rho_0\,(T)$ and bulk mean free path $\ell_0\,(T)$ appearing in any theory of size effects, represent *the resistivity and mean free path that would be observed at temperature T in a thin film where electron–surface scattering has been switched off*.

The calculation of the film resistivity at temperature T, $\rho(T)$, predicted by any of the theories of size effects (starting with FS), faces the severe practical difficulty that the ratio $\rho(T)/\rho_0(T) = [\sigma(T)/\sigma_0(T)]^{-1} = g(\delta, \xi, x)$ turns out to depend on the dimensionless parameter $x(T) = t/\ell_0\,(T)$—where $g(\delta, \xi, x) > 1$ is a function predicted by theory, that describes the increase in resistivity attributable to electron–surface scattering. Consequently, to calculate $\rho(T)$, we need to know $\rho_0(T)$ and $\ell_0\,(T)$ that characterize the bulk at temperature T, *and these parameters are not known a priori*.

To determine the unknown quantity ℓ_0 we imposed a condition of self-consistency: That ℓ_0 be such that the theoretical prediction (regardless of the theoretical model employed to describe size effects) coincides with experimental data at 4 K, temperature at which the contribution to the film resistivity arising from electron–phonon scattering is negligible because the phonons are frozen out. We plotted the function $\rho(4) = \rho_0[\ell_0\,(4)]g[\delta, \xi, x(4)] = (m \times v_F)/(nq^2)(g(\delta, \varsigma, x(4) = (\ell_0(4)/t))/\ell_0(4))$ as a function of the bulk mean free path $\ell_0\,(4)$ at 4 K, for each theory, employing the values of (δ, ξ) characterizing the rough surface *measured through*

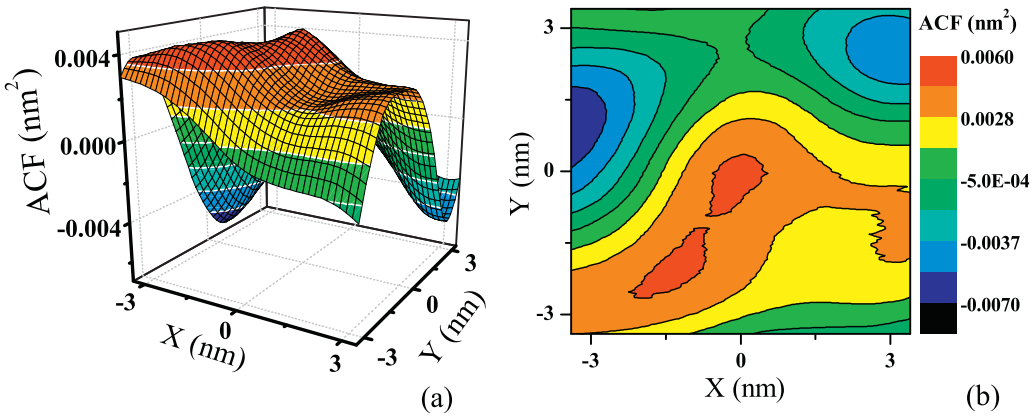

Fig. 3. (a) Three dimensional representation of the ACF data of one image of a grain terrace recorded with the STM on the 54 nm thick sample. (b) Two dimensional plot of the curves at different levels of the ACF data plotted in Fig. 4a.

independent experiments. From the plot we found the value of ℓ_0 (4) and the corresponding $\rho_0(4)$, that reproduces the residual resistivity $\rho(4)$ measured on each sample. The results coincide with those obtained following an iteration procedure already published [19,20]. This method of data analysis departs from the traditional method of data analysis used for several decades, *where ℓ_0 (T) and $\rho_0(T)$ have been assumed to be the same for a family of films of the same metal but of different thickness, prepared under similar conditions of evaporation*.

The bulk resistivity $\rho_0(4)$ obtained through this process allows an estimation of the bulk collision time $\tau_0(4) = m^*/(nq^2\rho_0(4))$, as well as the bulk resistivity ρ_0(T) and bulk mean free path ℓ_0 (T) at $T > 4$K. Increasing temperature T adds a statistically independent collision time $\tau(T)_{\text{EL-PHON}}$ due to electron–phonon scattering. The average time between collisions in the bulk at temperature $T > 4$ K, can be computed using the Bloch–Grüneisen theory following Matthiessen's rule: $1/\tau_0(T) = 1/\tau_0(4) + 1/\tau(T)_{\text{EL-PHON}}$. We computed $\tau(T)_{\text{EL-PHON}}$ from the values of the intrinsic resistivity $\rho_0(T)_{\text{EL-PHON}}$ (arising solely from electron–phonon scattering at temperature T) for crystalline gold [24].

The average distance traveled by an electron between collisions ℓ_0 (T) = $v_F\tau_0(T)$ computed in this way represents *the mean free path in the bulk, in a crystal having the same concentration of impurities/point defects as the thin film being measured (where electron–surface scattering has been switched off)*. The values of $\rho_0(4)$ emerging from data analysis involving different theoretical models are listed in Table 3. It seems clear that cooling the samples to 4 K increases ℓ_0 by roughly two orders of magnitude, from ℓ_0 (300) = 38 nm, to ℓ_0 (4) ≈ 1000 nm, therefore the range of $x(T)$ accessible in the experiment decreases by about two orders of magnitude.

3.3. Comparison between theories of size effects and thin film resistivity data

3.3.1. Classical Transport Theories

We discuss below, the predictions regarding transport theories that are based upon a classical description of electron motion provided by a BTE. Comparison between predictions based upon classical theories of size effects and resistivity data is displayed in Fig. 5, the increase in resistivity $\rho(T)/\rho_0(T)$ attributable to electron–surface scattering in the 54 nm thick film, are displayed in Fig. 6.

There are many classical theories of size effects published over several decades, where authors have introduced a variety of phenomenological parameters into solutions of the BTE. We restrict comparison between classical theories and experimental data only to the 3 most relevant classical models: (i) The very first model formulated by Drude in 1900 before the advent of Quantum Mechanics; (ii) the theory of Fuchs–Sondheimer, that is certainly the most influential theory of size effects, and (iii) the theory of Calecki, which is *the only classical theory where the effect of electron–surface scattering was included into the Boltzmann collision operator using no adjustable parameters*.

3.3.1.1. Drude's model. According to Drude's model, ℓ (T) = $v_F\tau(T)$. Cooling the sample freezes out phonons, so ℓ (4) represents the scale of distance characterizing defects that give rise to electron scattering at 4 K. From Table 1 we observe that ℓ (4) ≈ 2t, in agreement with Ref. [25].

As outlined in Section 3.2, increasing temperature T adds a statistically independent collision time $\tau(T)_{\text{EL-PHON}}$ due to electron–phonon scattering. The average time between collisions at temperature $T > 4$ K, can be computed following Matthiessen's rule: $1/\tau(T) = 1/\tau(4) + 1/\tau(T)_{\text{EL-PHON}}$, from the intrinsic resistivity of crystalline gold $\rho(T)_{\text{EL-PHON}}$ [24]. Drude's predictions for the resistivity of the thin gold films computed in this way are displayed in Fig. 5.

3.3.1.2. Fuchs–Sondheimer. The seminal work that guided research on size effects for several decades was the Fuchs–Sondheimer (FS) theory [14], a formalism where the motion of electrons in a metal film is described by a BTE. According to FS, the resistivity of a metallic film, is given by $\rho(T) = \rho_0(T)/[x(T)\,\varphi(s)]$, where $\rho_0(T)$ is the bulk resistivity described by a Bloch–Grüneisen law, $x(T) = t/\ell_0$ (T) [notice that ℓ_0 (T) stands for the electron mean free path at temperature T in the absence of electron–surface scattering], and $\varphi(s)$ (including two specularities P and Q that describe the fraction of electrons that undergo a specular reflection upon colliding with the two surfaces limiting the film), is defined by Eq. (2) in Ref. [26].

According to Table 1, in all four samples we observe ℓ (4) ≈ 2t, which reproduces results already reported in Table 1 of Ref. [25]. For this relation to hold, electrons colliding with one of the surfaces limiting the film must undergo a specular reflection [25,26]. Hence we used $P = 1$ to characterize the reflectivity of the mica. The fitting parameters left in the theory are Q (the specularity of the upper gold surface) and $\kappa(T)$.

To test Sondheimer's theory, we need to determine $x(T)$, hence ℓ_0 (T) at each temperature T. We determined ℓ_0 (T) as described in Section 3.2. The best description of the temperature dependence of the resistivity data is obtained for $Q = 0$ [22,27,28]. The result of the analysis following the Fuchs–Sondheimer's theory with $P = 1$ and $Q = 0$ for the 54 nm thick film is displayed in Fig. 5. Agreement

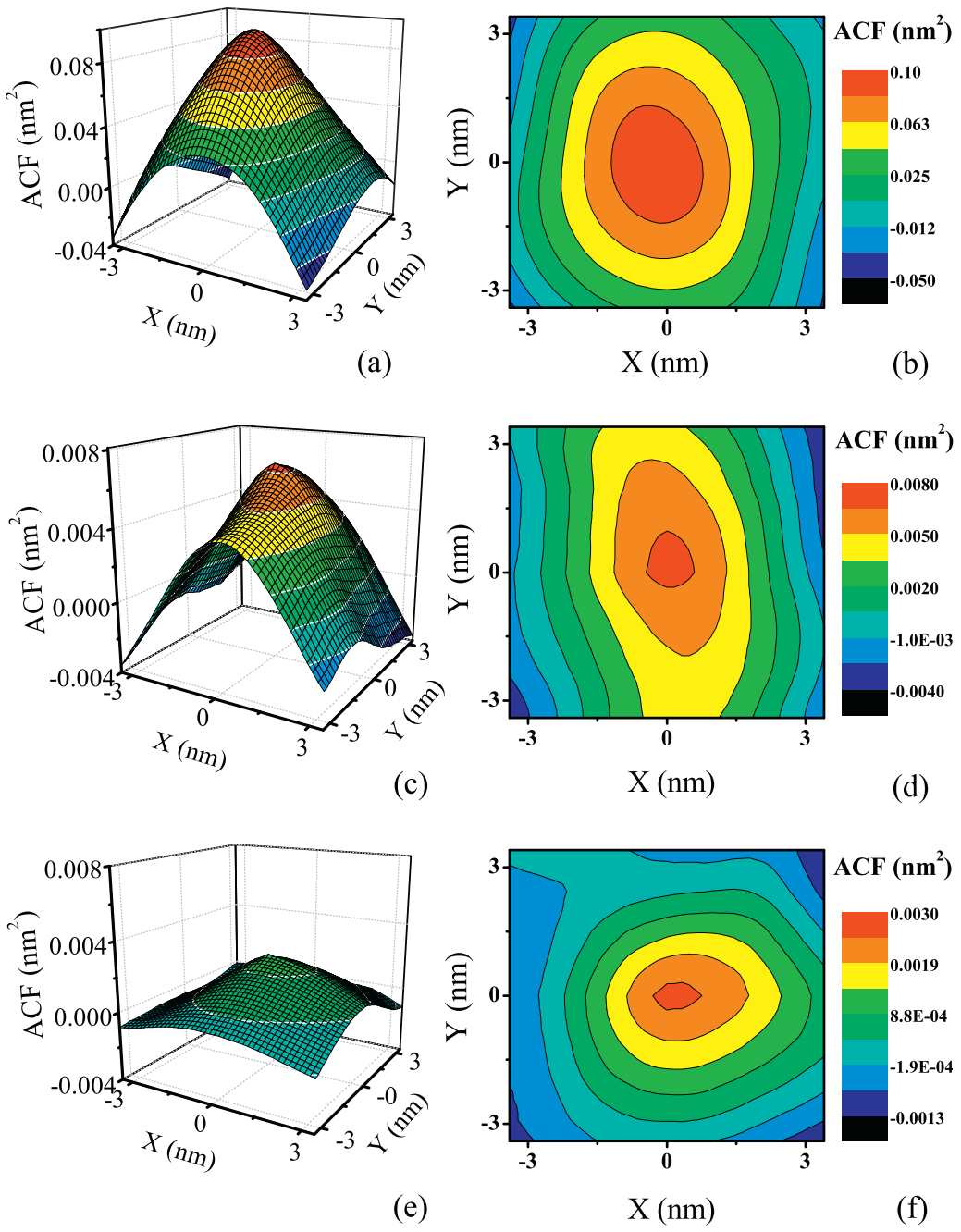

Fig. 4. Three dimensional representation of the ACF data averaged over 12 images of the (a) grain boundary, (c) grain side and (e) grain terrace of 12 random grains, and the two dimensional plot of the curves at different levels of the average ACF data from (b) grain boundary, (d) grain side and (f) grain terrace.

between theory and experiment obtained for $P = 1$ and $0 < Q < 1$ gets worse with increasing Q.

3.3.1.3. Calecki. Calecki's theory is also based upon BTE. And yet, it is the only classical theory that contains no adjustable parameters. The resistivity $\rho = (\sigma_0)^{-1}$ induced by electron–surface scattering can be univocally determined from the parameters (δ, ξ), where in this theory σ_0 is the conductivity coefficient defined by Eq. (32) in Ref. [15].

To compare theoretical predictions with experimental data, electron scattering by phonons and electron scattering by impurities/defects (the electron scattering mechanisms responsible for the bulk resistivity) must be added to electron–surface scattering predicted by theory, following the method described in Ref. [22]. The inverse of the relaxation time describing these processes, can be computed according to $1/\tau_0 = 1/\tau_{IMP} + 1/\tau_{EL\text{-}PHON}$, where the first (temperature-independent) term accounts for electron scattering by impurities, and the second (temperature-dependent) term accounts for electron–phonon scattering [26]. Following the procedure outlined in Section 3.2, we computed the collision time corresponding to electron-impurity scattering (Eq. (45) of Ref. [15]) and added the phonon contribution to determine the temperature dependence of the resistivity at temperatures T, $4\,K < T < 300\,K$. The temperature dependence of the resistivity predicted by Calecki's theory for the 54 nm film displayed in Fig. 5 was computed using the numerical solution of the transport equations contained in the model, involving no approximations, incorporating electron-scattering in the bulk in the manner described [26]. Predictions

Table 3
Residual resistivity $\rho(4)$. Experimental residual resistivity $\rho(4)$ corresponding to Drude's model, and theoretical residual resistivity $\rho_0(4)$ of the bulk, according to different models, considering the roughness parameters measured on different sites (GT, GS, GB). FS: Fuchs–Sondheimer [14], TJM: Tesanovic, Jaric and Maekawa [48], TA: Trivedi and Aschroft [49], mSXW: Modified theory of Sheng, Xing and Wang [16].

Site	t	$\rho_0(4)$ Drude	FS	Calecki	TJM	TA	mSXW
	t (nm)	(nΩ m)	(nΩ m)	(nΩ m)	(nΩ m)	(nΩ m)	(nΩ m)
GT	54	7.6	4.0	7.5	7.5	7.5	6.0
	96	4.1	2.1	4.1	4.0	4.1	3.1
	135	2.6	1.2	2.6	2.5	2.6	1.9
	255	1.7	0.9	1.7	1.6	1.6	1.0
GS	54	7.6	4.0	7.5	7.2	7.4	4.5
	96	4.1	2.1	4.1	4.0	4.0	2.9
	135	2.6	1.2	2.6	2.5	2.6	2.0
	255	1.7	0.9	1.7	1.6	1.6	1.1
GB	54	7.6	4.0	7.5	4.1	5.2	3.9
	96	4.1	2.1	4.1	2.0	2.6	2.2
	135	2.6	1.2	2.6	1.0	1.4	1.4
	255	1.7	0.9	1.7	0.8	1.0	1.0

of classical theories regarding the increase in resistivity $\rho(T)/\rho_0(T)$ attributable to electron–surface scattering are displayed in Fig. 6. In both Figs. 5–7 we used the roughness parameters (δ, ξ) determined at grain terraces (GT, Fig. 2, Table 2).

3.3.2. Quantum transport theories

The goal of theoretical research performed since the eighties, has been to build a formalism that would permit the prediction of the increase in resistivity due to size effects from first principles *without adjustable parameters*, simply from the information contained in the topography characterizing the rough surface.

3.3.2.1. Modified theory of Sheng, Xing and Wang. A significant step towards reaching this goal is the theory of Sheng, Xing and Wang (SXW) [29], that unifies the quantum transport theories then available, applicable to different special cases, with the classical FS formalism. SXW abandoned the model in which the motion of electrons is described via the classical BTE. They calculated instead the Green's function describing an electron gas confined within two potential barriers described by randomly rough surfaces. SXW

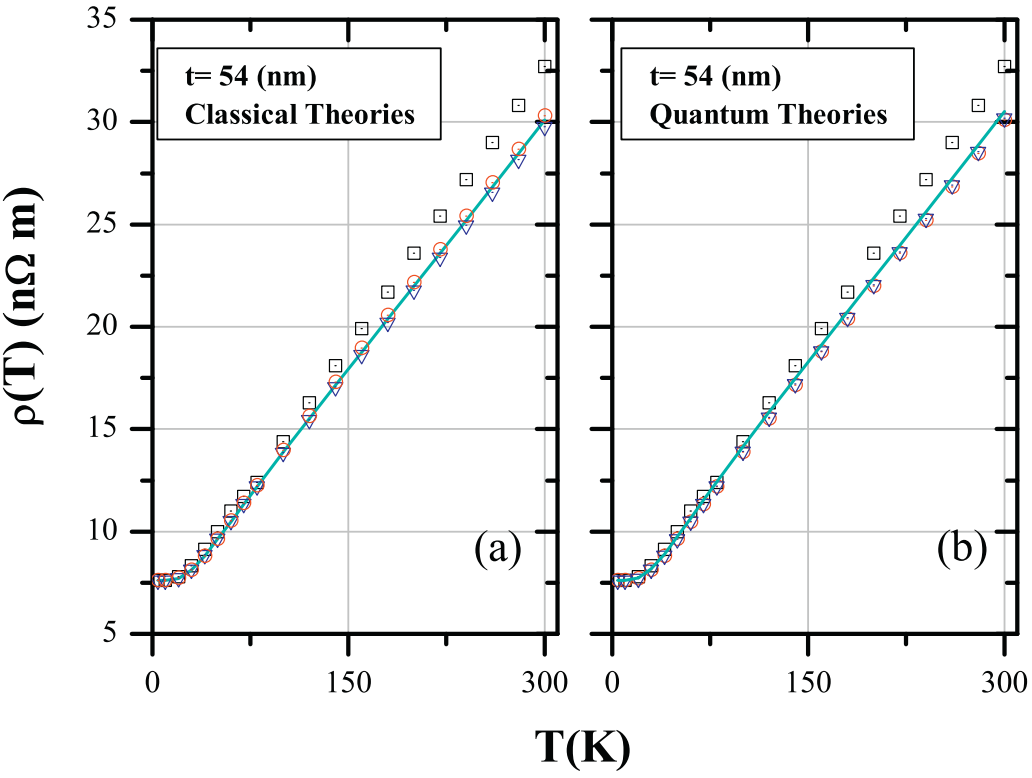

Fig. 5. Comparison of the temperature dependence of the resistivity data, for the sample 54 nm thick, with theoretical predictions based upon: (a) Classical transport theories: Black squares, experimental data. Green line, Drude. Blue-inverted triangle, Fuchs–Sondheimer. Red circle, Calecki. (b) Quantum transport theories: Black squares, experimental data. Red circle, TJM. Blue-inverted triangle, TA. Green line, mSXW, using the roughness parameters (δ, ξ) determined at grain terraces (GT, Fig. 2, Table 2). (For interpretation of the references to color in this figure legend, the reader is referred to the web version of the article.)

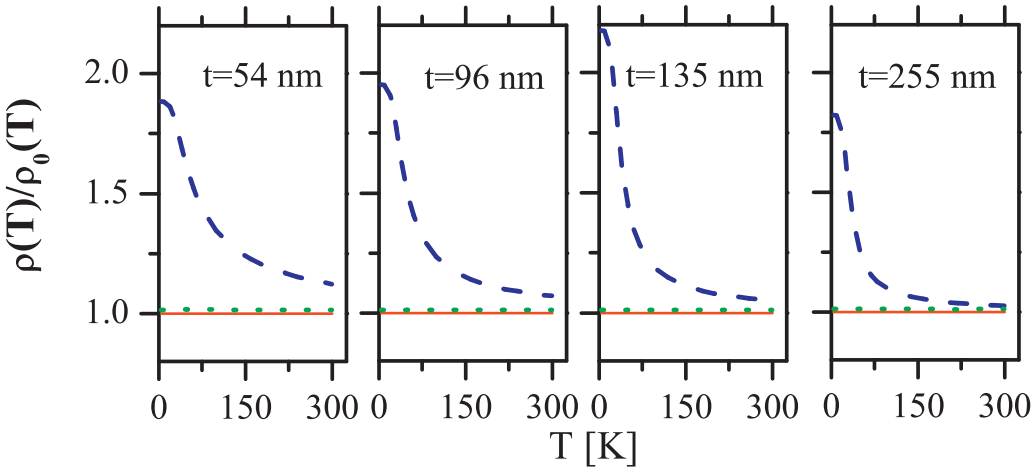

Fig. 6. Temperature dependence of $\rho(T)/\rho_0(T)$ predicted by different classical theories. Red line, Drude. Blue-dashed line, Fuchs–Sondheimer. Green-dotted line, Calecki, using the roughness parameters (δ, ξ) determined at grain terraces (GT, Fig. 2, Table 2). (For interpretation of the references to color in this figure legend, the reader is referred to the web version of the article.)

computed the dissipative part of the electron self-energy due to electron scattering by the rough surfaces using Dyson's equation, and proceeded to calculate the conductivity of the film using the Kubo transport formalism. SXW modeled the surface roughness by a white-noise surface profile, assuming that the height–height autocorrelation function (ACF) that on the average characterizes the rough surface is proportional to a Dirac's delta function, and hence its Fourier transform is a constant independent of the in-plane momentum of the electron.

An improved version of this model where the white noise approximation is abandoned, is the modified SXW theory (mSXW), that permits the calculation of both the quantum specularity function $R(\delta, \xi)$ and of the increase in resistivity attributable to electron–surface scattering, in films where the surface roughness is represented by an average ACF whose rms roughness amplitude is δ and its lateral correlation length is ξ, and the ACF is described either by a Gaussian or by an exponential [16].

The mSXW theory can be considered the quantum version of the FS theory, for it goes over into the FS formalism if the quantum specularity function $R(\delta, \xi)$ is replaced by a constant P, and the summation over a large number of sub bands (many sub bands occurs when $t \gg \lambda_F$) contained in the theory is replaced by an integral. Most important, is that the mSXW model permits the calculation of the ratio of film conductivity σ to bulk conductivity σ_0 attributable to electron–surface scattering, in terms of (δ, ξ) that characterize the roughness of the surface over a nanoscopic scale, *which are no longer adjustable parameters, but can be measured with a STM*.

The mSXW resistivity was computed as the inverse of the conductivity given by Eqs. (1) and (5) of Ref. [16]. The temperature dependence of the resistivity predicted by mSXW theory for the 54 nm thick film is displayed in Fig. 5; theoretical predictions of $\rho(T)/\rho_0(T)$ are displayed in Fig. 7.

Since the predicted increase in resistivity depends on the film thickness and on the parameters chosen to describe the rough surface, we performed the calculation for each of the different theoretical models, for each sample, employing the parameters (δ, ξ) corresponding to grain terraces (GT), to grain sides (GS) and to grain boundaries (GB) displayed in Fig. 2 and listed in Table 2 as well. The results of the data analysis, over each site, regarding the predicted temperature dependence of the film resistivity and the agreement with experimental values, are similar to what is reported in Fig. 5. The residual bulk resistivity $\rho_0(4)$ corresponding to each model, considering the roughness parameters measured on different sites (GT, GS, GB), are displayed in Table 3. The residual bulk resistivity corresponding to each film varies for the same model and for different values of (δ, ξ) characterizing each sample.

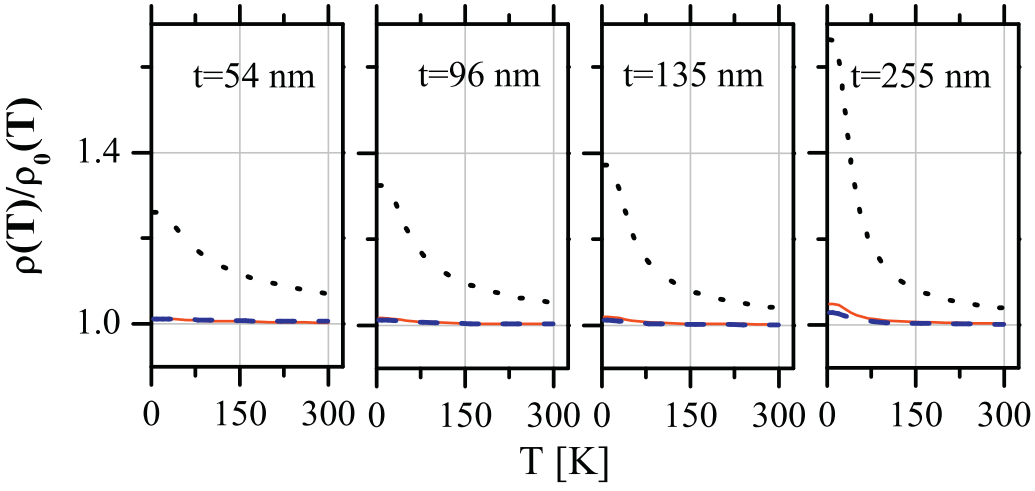

Fig. 7. Temperature dependence of $\rho(T)/\rho_0(T)$ predicted by different quantum theories. Red line, TJM. Blue-dashed line, TA. Black-dotted line, mSXW, using the roughness parameters (δ, ξ) determined at grain terraces (GT, Fig. 2, Table 2). (For interpretation of the references to color in this figure legend, the reader is referred to the web version of the article.)

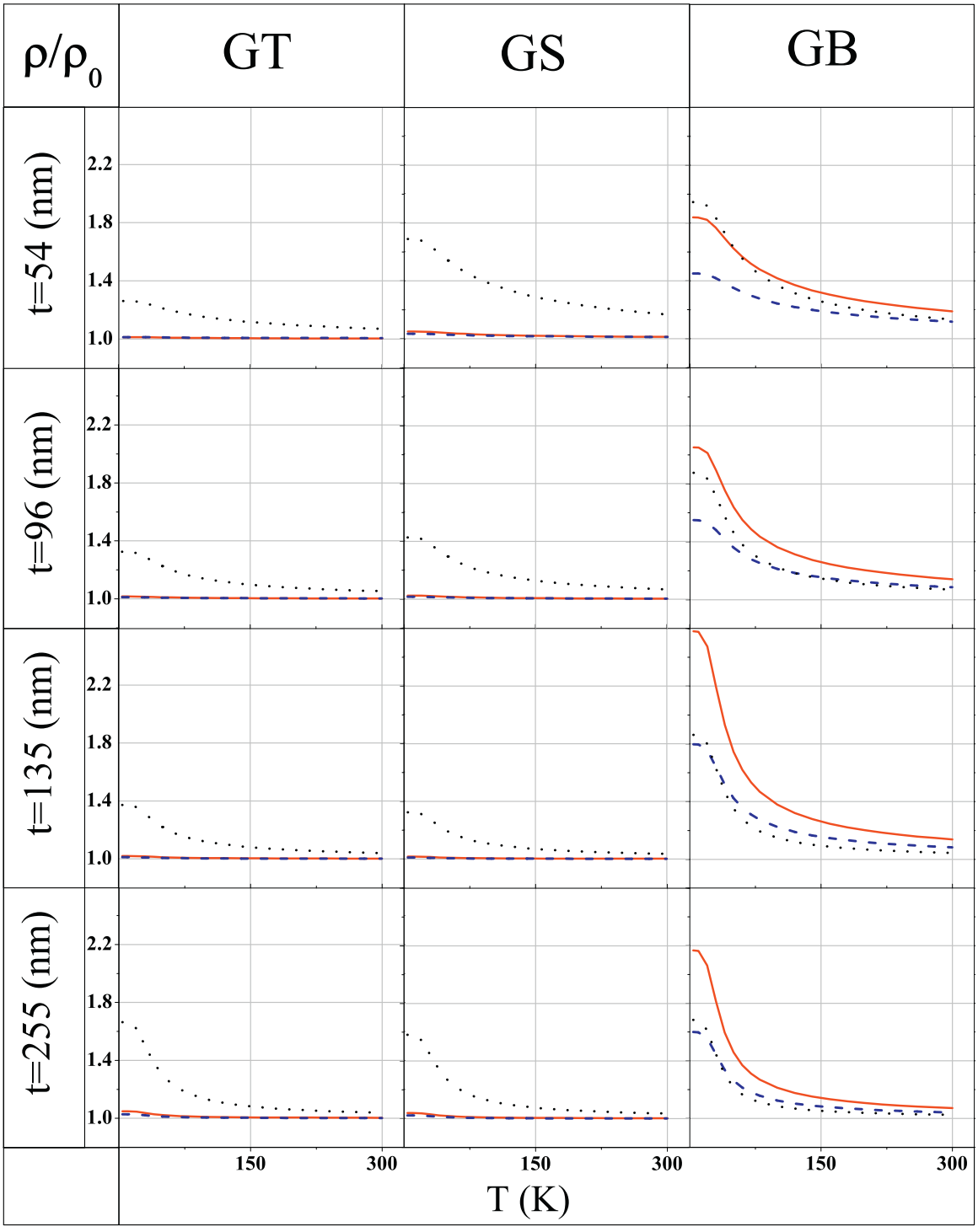

Fig. 8. Comparison of the temperature dependence of ρ/ρ_0 for each sample, according to different quantum models, considering the roughness parameters measured on different sites: grain terraces (GT, Fig. 2, Table 2), grain side (GS, Fig. 2, Table 2), grain boundary (GB, Fig. 2, Table 2). Theoretical predictions based upon: Red line, TJM. Blue-dashed line, TA. Black-dotted line, mSXW. (For interpretation of the references to color in this figure legend, the reader is referred to the web version of the article.)

Comparison between predictions concerning the *increase* in resistivity $\rho(T)/\rho_0(T)$ attributable to electron–surface scattering based upon different quantum transport theories, using the roughness parameters (δ, ξ) determined at different sites (GT, GS or GB), are displayed in Fig. 8.

Beyond the mSXW model, there are several quantum transport theories that have been published, some of which are listed in Refs. [30–49]. A feature common to quantum transport theories, is that the resistivity ρ_{AB} arising from two electron scattering mechanisms A and B acting together, is not the sum of the resistivities $\rho_A + \rho_B$, where ρ_A and ρ_B is the resistivity that would be observed if only mechanism A or mechanism B were active in the specimen. The rule $\rho_{AB} = \rho_A + \rho_B$ is known as Mathiessen's rule. The theoretical foundation underlying Mathiessen's rule arises from a classical description of electron motion based upon BTE, and upon solutions of BTE where the relaxation time approximation is used to describe the effect of different electron scattering mechanisms.

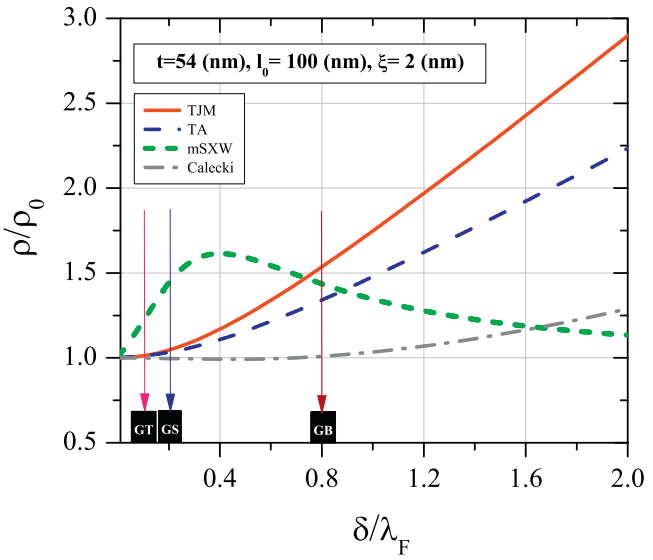

Fig. 9. Comparison between the predictions of different quantum transport theories in the 54 nm thick film, regarding the dependence of the increase in resistivity ρ/ρ_0 on the scale of distances involved in electron–surface scattering, determined by δ, the rms roughness amplitude of the Gaussian autocorrelation function, measured in units of the Fermi wave length for Au ($\lambda_F = 0.52$ nm). Typical (representative) values of $\xi = 2.00$ nm, and $\ell_0 = 100$ nm, were used. Solid red line, TJM. Dashed-blue line, TA. Dashed-green line, mSXW. Dashed-dotted grey line, Calecki. (For interpretation of the references to color in this figure legend, the reader is referred to the web version of the article.)

It seems interesting to note that, as a consequence of Calecki's formalism (based upon BTE), it turns out that effect of electron–surface scattering within the Boltzmann collision operator *cannot be represented by a relaxation time, for a relaxation time does not exist* (unless the metallic film is so thin that there is only one occupied sub band) [15]. Consequently, once this classical description of electron motion based upon solutions of BTE employing a relaxation time is abandoned, it is natural to expect violations of Mathiessen's rule, when one of the relevant electron scattering mechanisms is electron–surface scattering. The electron scattering mechanisms relevant to this problem at 4 K, are electron–surface and electron-impurity/defect scattering. Within the context of size effects, violations of this rule at 4 K are caused by interference between electron–surface and electron-impurity scattering, a subject that has been discussed recently [36]. All quantum transport theories of size effects considered in the data analysis and in the discussion are known to violate Mathiessen's rule at 4 K [50].

Out of many quantum theories that have been published, some of which are listed in Refs. [29–48], we restrict comparison between theory and experiment only to those theories that lead to a film conductivity σ that can be computed directly from the bulk conductivity σ_0, and from the parameters (δ, ξ) characterizing a Gaussian ACF describing the rough surface. The bulk mean free path ℓ_0 (T) corresponding to each theory was determined as described in Section 3.2.

The ability of different quantum theories of size effects to select the appropriate scale of distances relevant for describing electron–surface scattering is displayed in Fig. 9.

3.3.2.2. Tesanovic, Jaric and Maekawa. Tesanovic, Jaric and Maekawa (TJM) published a calculation of the increase in resistivity arising from electron–surface scattering, for a metallic film bounded by rough surfaces [48]. They considered that the electron gas confined within two rough surfaces has an energy H that is almost the same as the energy H_0 of the electron gas confined within two parallel flat plates, and that $H - H_0$ can be treated as a perturbation with respect to H_0. They developed a perturbation expansion for the "effective" Hamiltonian, using a non-unitary transformation. The authors computed the Green's function corresponding to this effective Hamiltonian, and calculated the conductivity of the film from first principles, using the Kubo linear response theory. The effective Hamiltonian induces sub band mixing over the unperturbed eigenstates of H_0. In their calculation they used the white noise approximation to describe the surface roughness.

Using this formalism, we computed the resistivity of the films as the inverse of the conductivity given by Eq. (7) of Ref. [48]; theoretical predictions of $\rho(T)/\rho_0(T)$ are displayed in Fig. 7.

3.3.2.3. Trivedi and Aschroft. Trivedi and Aschroft (TA) published a calculation of the increase in resistivity arising from electron–surface scattering for a metallic film bounded by rough surfaces that also proceeds from first principles [49]. They developed a perturbation expansion for the effective Hamiltonian, using a non-unitary transformation that can be understood as a transformation that flattens out the rough surface, similar to that used by TJM. They computed the matrix elements of the perturbation Hamiltonian, and they computed the conductivity of the film using the white noise approximation to describe the surface roughness. They also found that the rough surface scatters electrons belonging to different unperturbed eigenstates of H_0. The resistivity of the films was computed as the inverse of the conductivity given by Eq. (4.13) of Ref. [49]; theoretical predictions of $\rho(T)/\rho_0(T)$ are displayed in Fig. 7.

4. Results

The resistivity of the 4 samples is ordered such that it decreases with increasing thickness, at temperatures T such that $4\,K < T < 300\,K$. The samples exhibit a resistivity $\rho(300)$ that is a few percent in excess of the resistivity of 22.5 nΩ m expected from electron–phonon scattering, the electron scattering mechanism dominant in high purity crystalline gold at 300 K. The excess resistivity (with respect to the resistivity of high purity crystalline gold at 300 K) ranges from 3.5% for the thickest (255 nm), to 45% for the thinnest (54 nm) sample. The resistivity at 4 K decreases with increasing thickness. Cooling to 4 K decreases the resistivity of the films by one order of magnitude, leading to a $\rho(4)$ that differs by over a factor of 4 between the thinnest and the thickest film, in spite of the fact that the corresponding $\rho(300)$ do not differ by more than 40%. At temperatures in the neighborhood of 300 K, the slope $d\rho/dT$ decreases with increasing film thickness.

We varied the range of film thickness from $t = 54$ nm to $t = 255$ nm, hence the dimensionless ratio $x(T) = t/\ell_0\,(T)$ initially ranges from $1.4 < x(300) < 6.8$ at 300 K, where t is the film thickness and $\ell_0\,(T)$ is the electronic mean free path in the bulk at temperature T. As shown below, cooling the samples to 4 K increases $\ell_0\,(T)$ by about two orders of magnitude, therefore at temperatures in the neighborhood of 4 K, we reach a regime where $x(T) < 1$, that warrants the dominance of electron–surface scattering on the observed resistivity. Since the importance of electron–surface scattering relative to electron–phonon/impurity scattering depends on $x(T)$, lowering the temperature T induces an effect that should be equivalent to decreasing sample thickness. The resistivity data reported in this paper covers approximately the range $0.1 < x(T) < 6.8$, for $4\,K < T < 300\,K$.

XRD data point to the fact that the samples exhibit grains oriented such that direction <1 1 1> of gold is perpendicular to the surface of the mica. The (cleaved) surface of the mica consists of atomically flat areas limited by cleavage steps separated by distances of several hundred nanometers, as imaged with an AFM. As a

Table 4
Goodness of the theoretical description of the resistivity $\rho(T)$. Goodness of the theoretical description of the resistivity, computed as $\chi_1{}^2 = \sum_{j=1}^{N}(\rho_{EXP}(T_j) - \rho_{THEO}(T_j))^2/(\rho_{THEO}(T_j))$, where $N=20$ is the number of data points at different temperatures T_j; $\rho_{EXP}(T_j)$ and $\rho_{THEO}(T_j)$ are the experimental and theoretical resistivity at $T=T_j$.

Sample t (nm)	$\chi_1{}^2$ Drude (nΩ m)	FS (nΩ m)	Calecki (nΩ m)	TJM (nΩ m)	TA (nΩ m)	mSXW (nΩ m)
54	1.3	1.5	1.0	1.3	1.2	0.7
96	3.9	4.3	3.5	3.9	3.8	2.9
135	0.5	0.7	0.4	0.5	0.5	0.1
255	0.1	0.1	0.2	0.1	0.1	0.3

consequence of the sample preparation method, the grain diameter D does not seem to depend on sample thickness.

5. Discussion

During the last few years we published the measurement of galvanomagnetic phenomena arising from electron–surface scattering at low temperatures that will be used in the Discussion to discriminate predictions based upon different theories of size effects. We published the first measurement of the Hall effect [23] and the Hall constant [26], of the transverse magnetoresistance [27,28], and of the longitudinal magnetoresistance [25], *where the signal at 4 K arises univocally from electron–surface scattering*.

The measurement of magnetomorphic effects arising from electron–surface scattering constitute a powerful experimental tool that allows an identification of different microscopic electron scattering mechanisms. In fact, when electron–surface scattering is the dominant electron scattering mechanism at 4 K, then both the Hall mobility $\mu_H(4)$ (which is proportional to the average electronic collision time) depends linearly on film thickness [23], and the transverse as well as the longitudinal magnetoresistance observed at 4 K and 9 T increases with increasing film thickness [25,27]. However, when the temperature of the samples increases to some 50 K, the Hall mobility decreases by over a factor of two [23], and the transverse magnetoresistance [27] as well as the longitudinal magnetoresistance [25] observed at 9 T decreases by over a factor of four. This indicates that *at 50 K, electron–phonon scattering (instead of electron–surface scattering) takes over as the dominant electron scattering mechanism.*

Within this broad context of charge transport and size effects that includes resistivity as well as galvanomagnetic phenomena arising from electron–surface scattering, there are several interesting consequences that emerge from the work reported here:

5.1. Predicting Power of theories of size effects

The theories of size effects do exhibit a predicting power, in the sense that we can roughly estimate (to within 10%, regardless of the film thickness) what the resistivity of a thin metallic film would be at different temperatures, from the typical parameters that characterize the average surface roughness, that could be measured routinely with an AFM/STM endowed with atomic resolution. The accuracy with which the resistivity can be predicted for different film thickness using different theories is displayed in Table 4. The predicted resistivity turns out to be almost independent of the site chosen to measure the surface roughness parameters (δ, ξ): grain terrace, grain side, or grain boundary. However, the increase in resistivity $\rho(T)/\rho_0(T)$ attributable to electron–surface scattering turns out to depend on the site chosen to measure the roughness parameters (δ, ξ), and it turns out to be model-dependent.

5.2. Residual bulk resistivity

As displayed in Table 3, regardless of which theoretical model we choose, the residual bulk resistivity corresponding to each sample turns out to depend on film thickness, *a result that is at variance with the central assumption used for decades to analyze thin film resistivity data.* This can be considered a severe warning regarding the applicability of resistivity data analysis based upon parameter fitting performed over many decades. Not only because electron-grain boundary scattering may have contributed a significant amount to the observed resistivity data reported by many other authors, but because such data analysis is based upon a simplifying assumption *whose validity seems questionable: the assumption that the parameters characterizing the bulk, for a family of films of the same metal prepared under similar conditions of evaporation, are independent of film thickness.* A bulk resistivity that varies with film thickness may be understood as arising from a concentration of impurities/defects present in the samples that varies with film thickness. The residual resistivity observed in crystalline samples is known to depend on the impurity/defect concentration [24].

5.3. Drude's model

The accuracy of the temperature dependence of the resistivity predicted by Drude's model published in 1900, seems remarkably comparable to the predictions based upon models published several decades later, such as Fuchs–Sondheimer (1950), Tesanovic, Jaric and Maekawa (1986), Trivedi and Aschroft (1988), Calecki (1990), and the modified theory of Sheng, Xing and Wang (1999).

5.4. Increment in resistivity predicted by different models

The resistivities predicted by different models, either classical or quantum, including Drude's, are in rough agreement with the experimental values and with each other, regardless of the site chosen to measure the surface roughness parameters (δ, ξ). As expected, the increase of resistivity of the thin film attributable to electron–surface scattering is largest at 4 K, and decreases with increasing temperature, but varies between different models. The resistivity ratio ρ/ρ_0 predicted by FS turns out to be the largest, as the increment in resistivity arising from electron–surface scattering turns out to be of the order of 80% to 120% at 4 K. The increment in resistivity at 4 K predicted by mSXW varies between 30% and 80%. By contrast, the temperature dependence of the resistivity predicted by Calecki's theory agrees roughly with that predicted by Drude's model, and the increment in resistivity ρ/ρ_0 predicted by Calecki is merely of the order of one percent or smaller at 4 K, independently of the site under analysis: grain terrace, grain side or grain boundary. As depicted in Fig. 8, the increase in resistivity predicted by TJM and TA at 4 K also turns out to be of the order of a few percent, unless the roughness parameters (δ, ξ) are measured at grain boundaries.

5.5. Electron-surface scattering and magnetomorphic effects

The small increase in resistivity at 4 K (of order a few %) induced by electron–surface scattering predicted by the TJM and TA models, when using the surface roughness measured at grain terraces or grain sides, and the small increase (less than 1%) predicted by Calecki at any site, are in contradiction with measurements of magnetomorphic coefficients at low temperatures: The temperature dependence of the Hall mobility μ_H(T), of the transverse magnetoresistance and of the longitudinal magnetoresistance $(\Delta\rho/\rho)$(T). For at 4 K, $\mu_H(4)$ depends linearly on film thickness, and the transverse as well as the longitudinal $(\Delta\rho/\rho)(4)$ measured at 9 T also increases with increasing film thickness t, signaling the predominance of electron–surface scattering at 4 K. Increasing T to 50 K results in a decrease of $\mu_H(50)$ by over a factor of two [23], while the transverse [27] and the longitudinal $(\Delta\rho/\rho)(50)$ decreases by about a factor of four [25], indicating that at 50 K *electron–phonon scattering becomes the dominant scattering mechanism*. The fact that, based upon the measurement of these magnetomorphic effects, *electron–surface scattering dominates charge transport at 4 K but is no longer dominant at 50 K*, contradicts the small variation of the ratio $\rho(T)/\rho_0(T)$ with respect to unity between 4 K and 300 K, predicted by Calecki, TA and TJM. The theories that do predict a variation of $\rho(T)/\rho_0(T)$ that would seem consistent with the measurement of these magnetomorphic effects, are the classical Sondheimer model and its quantum version, the mSXW theory.

5.6. Scale of distances relevant for electron-surface scattering

The ratio ρ/ρ_0 predicted by different theories exhibits a markedly different dependence on the scale of length involving electron–surface scattering (that is reflected on the dependence of the ratio ρ/ρ_0 on the rms amplitude δ of the Gaussian describing the ACF, that in turn depends on the scale of distances over which corrugations are measured). While the models TA, TJM and Calecki predict a monotonic increase of the ratio ρ/ρ_0 with increasing δ, the mSXW turns out to be the only model that predicts an increase in resistivity that takes on its maximum value at around $\delta/\lambda_F \approx 0.4$ (for $\xi = 2.0$ nm) and then decreases with increasing δ (Fig. 9). This confirms our earlier preliminary finding [17].

6. Conclusions and summary

In this work, we report the comparison between the resistivity measured on a family of thin gold films, with predictions based upon classical theories of size effects (Drude's, Sondheimer's and Calecki's), as well as predictions based upon quantum theories of electron–surface scattering (Trivedi and Aschroft, Tesanovic, Jaric and Maekawa, and the modified theory of Sheng, Xing and Wang). The temperature dependence of the resistivity was measured on four gold films of different thickness evaporated onto preheated mica substrates, between 4 K and 300 K. The resistivity data reported in this paper covers approximately the range $0.1 < x(T) < 6.8$, for $4\,K < T < 300\,K$, where $x(T)$ is the ratio between film thickness and electron mean free path in the bulk at temperature T. We experimentally identify electron–surface and electron–phonon scattering as the microscopic electron scattering mechanism giving rise to the macroscopic resistivity observed in our samples. The morphology of the samples was examined using XRD, RBS and STM. From images recorded with the STM on each sample, we determined the rms roughness amplitude δ and the lateral correlation length ξ corresponding to a Gaussian representation of the average height–height autocorrelation function, measured over the scale of length set by the Fermi wave length. Using (δ, ξ) as input data, we present the first rigorous comparison of thin film resistivity data with predictions based upon the theory of Calecki and with quantum theoretical predictions using *no adjustable parameters*.

The different theories are all capable of estimating the thin film resistivity at temperature T ($4\,K < T < 300\,K$) to an accuracy better than 10%. The mean free path and the resistivity characterizing the bulk *do depend on film thickness*, a result at variance with the central assumption that has been used for several decades to analyze thin film resistivity data. However, only the Sondheimer theory and its quantum version, the modified theory of Sheng, Xing and Wang, predict an increase in resistivity arising from size effects that seems to be consistent with galvanomagnetic phenomena arising from electron–surface scattering measured at low temperatures.

Acknowledgments

We gratefully acknowledge funding from FONDECYT under contract 1085026. M. Flores thanks PSD53 project.

References

[1] I. Stone, Phys. Rev. 6 (1898) 1.
[2] The ITRS (International Technology Roadmap for Semiconductors) is a report published periodically by the semiconductor industry. The debate over the increase in resistivity arising from structural defects on Cu lines connecting transistors in an integrated circuit, has been included in ITRS reports at least since 1999, www.itrs.net/links/.
[3] M. Wang, et al., J. Mater. Sci. Technol. 25 (2009) 699.
[4] Q. Huang, et al., Appl. Phys. Lett. 95 (2009) 103112.
[5] Y. Kitaoka, et al., Appl. Phys. Lett. 95 (2009) 052110.
[6] J.S. Chawla, D. Gall, Appl. Phys. Lett. 94 (2009) 252101.
[7] P. Ercius, et al., Microsc. Microanal. 15 (2009) 244.
[8] A.E. Yarimbiyik, et al., Microelectron. Reliability 49 (2009) 127.
[9] R.L. Graham, et al., Appl. Phys. Lett. 96 (2010) 042116.
[10] T. Sun, et al., Phys. Rev. B79 (2009) 041402.
[11] T. Sun, et al., Phys. Rev. B81 (2010) 155454.
[12] This is reflected on the increase in resistivity arising from structural defects at 300 K [above the bulk resistivity $\rho_0(300) = 17\,n\Omega\,m$ of crystalline Cu], of Cu lines connecting the transistors making up an integrated circuit. For lines whose half-pitch is 35 nm, in 2002 this increase was estimated to be between 30% and 55% [P. Kappur et al., IEEE Trans. Elect. Devices 49 (2002) 590, Fig. 10a]. The estimation was revised upwards to approximately 100% three years later (Ref. [2], ITRS Interconnect 2005 and 2007).
[13] P.M.Th.M. Van Attekum, et al., Phys. Rev. B29 (1984) 645.
[14] E.H. Sondheimer, Adv. Phys. 1 (1950) 1.
[15] D. Calecki, Phys. Rev. B42 (1990) 6906.
[16] R.C. Munoz, et al., J. Phys.: Condens. Matter 11 (1999) L299.
[17] R.C. Munoz, et al., Phys. Rev. B 62 (2000) 4686.
[18] R.C. Munoz, et al., J. Phys.: Condens. Matter 12 (2000) 2903.
[19] R.C. Munoz, et al., J. Phys.: Condens. Matter 12 (2000) L379.
[20] R.C. Munoz, et al., J. Mol. Catal. A 228 (2005) 163.
[21] G. Kastle, et al., Phys. Rev. B70 (2004) 165414.
[22] R. Henriquez, et al., Phys. Rev. B82 (2010) 113409.
[23] R.C. Munoz, et al., Phys. Rev. Lett. 96 (2006) 206803.
[24] R.A. Matula, J. Phys. Chem. Ref. Data 8 (1979) 1147.
[25] R.C. Munoz, et al., Phys. Rev. B 81 (2010) 165408.
[26] R. Henriquez, et al., J. Appl. Phys. 108 (2010) 123704.
[27] R.C. Munoz, et al., J. Phys.: Condens. Matter 18 (2006) 3401.
[28] R.C. Munoz, et al., Phys. Rev. B 74 (2006) 233402.
[29] L. Sheng, D.Y. Xing, Z.D. Wang, Phys. Rev. B51 (1995) 7325.
[30] A.E. Meyerovich, S. Stepaniants, Phys. Rev. B51 (1995) 17116.
[31] A.E. Meyerovich, S. Stepaniants, Phys. Rev. B 58 (1998) 13242.
[32] A.E. Meyerovich, S. Stepaniants, Phys. Rev. B 60 (1999) 9129.
[33] A.E. Meyerovich, S. Stepaniants, J. Phys.: Condens. Matter 12 (2000) 5575.
[34] A.E. Meyerovich, L.V. Ponomarev, Phys. Rev. B 65 (2002) 155413.
[35] A.E. Meyerovich, L.V. Ponomarev, Phys. Rev. B67 (2003) 165411.
[36] S. Chatterjee, A.E. Meyerovich, Phys. Rev. B81 (2010) 245409.
[37] G. Palasantzas, J. Barnas, J. Phys. Rev. B 56 (1997) 7726.
[38] G. Palasantzas, J. Barnas, Phys. Sat. Sol. B211 (1999) 671.
[39] G. Palasantzas, Phys. Rev. B 58 (1998) 9685.
[40] G. Palasantzas, et al., Phys. Rev. B61 (2000) 11109.
[41] G. Palasantzas, T.J.M. De Hosson, Phys. Rev. B63 (2001) 125404.
[42] G. Palasantzas, T.J.M. De Hosson, J. Appl. Phys. 93 (2003) 320.
[43] G. Palasantzas, et al., Surf. Sci. 507 (2002) 541.
[44] K.M. Leung, Phys. Rev. B30 (1984) 647.
[45] C.S. Chu, R.S. Sorbello, Phys. Rev. B38 (1988) 7260.
[46] G.Z. Zhang, W.H. Butler, Phys. Rev. B51 (1995) 10085.
[47] Z. Tesanovic, et al., Phys. Rev. Lett. 57 (1987) 2760.
[48] Z. Tesanovic, J. Phys. C: Solid State Phys. 20 (1987) L829.
[49] N. Trivedi, N.W. Aschroft, Phys. Rev. B38 (1988) 12298.
[50] R.C. Munoz, et al., J. Phys.: Condens. Matter 15 (2003) L177.